A New Class of Chaotic Attractors in Murali-Lakshmanan-Chua Circuit

ALI OKSASOGLU*

Honeywell Corporation, 11100 N. Oracle Rd., Tucson, AZ 85737.

QIUDONG WANG†

Department of Mathematics, The University of Arizona, Tucson, AZ 85721.

Abstract

In this paper, we study the existence of a new class of chaotic attractors, namely the rank one attractors, in the MLC (Murali-Lakshmanan-Chua) circuit [Murali *et al.*, 1994b] by numerical simulations based on a theory of rank one maps developed in [Wang & Young, 2005]. With the guidance of the theory in [Wang & Young, 2005], weakly stable limit cycles, found through Hopf bifurcations and other numerical means, are subjected to periodic pulses with long relaxation periods to produce rank one attractors. The periodic pulses are applied directly as an input. Periodic pulses have been used before in various schemes of chaos. However, for this scheme of creating rank one attractors to work, the applied periodic pulses must have short pulse widths and long relaxation periods. This is one of the key components in creating this new class of chaotic attractors.

*Email: ali.oksasoglu@honeywell.com.

†Email: dwang@math.arizona.edu.

This research is partially supported by a grant from NSF.

1 Introduction

In this paper, we continue the study conducted in [Wang & Oksasoglu, 2005], where the authors introduced periodic kicking forces in Chua's circuit to create chaotic rank one attractors. These chaotic attractors are fractals of complicated geometric structure, dynamically characterized by positive Lyapunov exponents along typical orbits. They are numerically observable yet sensitive to perturbations. Our studies are motivated by a recent mathematical theory of rank one maps [Wang & Young, 2001, 2005].

The theory of rank one maps is originated from the studies of the logistic family ($f_a = 1 - ax^2$) and the Hénon family ($x_1 = 1 - ax^2 + y, y_1 = bx$). It is a result of a long and sustained effort on pushing chaos theory beyond the category of uniformly hyperbolic systems and horseshoe maps. Among the most important mathematical breakthroughs along the way are (1) Jakobson's theory of unimodal maps [Jakobson, 1981], (2) Benedicks' and Carleson's theory on the Hénon maps [Benedicks & Carleson, 1991] and the proof of Benedicks and Young on the existence of Sinai-Ruelle-Bowen (SRB) measure for good Hénon maps [Benedicks & Young, 1993]. In [Wang & Young, 2001, 2005], these developments are exploited in the study of attractors with a single direction of instability resulting recently in a general theory of rank one attractors.

In [Wang & Young, 2002b], the authors studied systems of ordinary differential equations of the form

$$\frac{d\mathbf{u}}{dt} = f(\mathbf{u}) + \varepsilon\Phi(\mathbf{u})P_T(t) \tag{1}$$

where $\mathbf{u} \in \mathbb{R}^m, m \geq 2$, and the second term on the right is a forcing term added to the original system defined by $f(\mathbf{u})$. They observed that, if the forcing term represents a periodic kick, then the time-T map of Eq. (1) in a small neighborhood of a weakly stable limit cycle of the unforced system (i.e., $\varepsilon = 0$) is, in general, a rank one map and the theory developed in [Wang & Young, 2001, 2005] apply. In [Wang & Young, 2004], chaotic attractors created by periodically kicking the weakly stable limit cycles emerging from a supercritical Hopf bifurcation are investigated.

In [Wang & Oksasoglu, 2005], the authors studied a concrete system for the applications of this theory. Periodic kicks were applied to the well-known Chua's circuit [Chua *et al.*, 1986; Madan, 1993] to create rank one attractors around the parameters of Hopf bifurcation. In the case of Chua's circuit, impulse and a pulse trains for $P_T(t)$ were employed along with a specific choice of $\Phi(\mathbf{u}) = (x, 0, 0)$.

In this paper, we study a second-order system whose governing equations can be obtained from the so-called MLC (Murali-Lakshmanan-Chua) [Murali *et al.*, 1994b,a] circuit shown in Fig. 1. In [Wang & Oksasoglu, 2005], the forcing term was a function of the phase variables, hence its physical implementation would require additions to the original circuit. In this paper, we set $\Phi(\mathbf{u}) = (1, 0)$ so that a periodic pulse can be directly applied as an input as shown in Fig. 1. Note that $\Phi(\mathbf{u})$ has a direct impact on the shape of the attractor. Our numerical investigation is also extended to periodic solutions other than those obtained from supercritical Hopf bifurcations, a case for which the corresponding theoretical computations are not available. At this point, it is worth noting that periodic pulses have been used numerous times before in the context of various chaotic schemes (e.g., see [Stojanovski *et al.*, 1996; Yang & Chua, 1997; Elwakil, 2002; Miyachi *et al.*, 2003; Özoguz & Elwakil, 2004]). However, the periodic pulses used in this investigation are characterized by a short pulse width followed by a long relaxation period. This type of pulses is employed to fulfil the recipe-like requirements of the theory of rank one maps in creating strange attractors.

We refer the reader to the first two sections of [Wang & Oksasoglu, 2005] for a brief discussion on the mathematical aspects of the theory of rank one attractors and a heuristic description of the mechanism by which rank one attractors are created. The content of rest of this paper is organized as follows: In Sec. 2, we make relevant theoretical computations for the case of Hopf limit cycles. The results of our numerical simulations for this case are given in Sec. 3. Section 4 covers some ground for additional considerations, namely, the case of periodic pulses of sinusoidal shape, and the non-Hopf limit cycles.

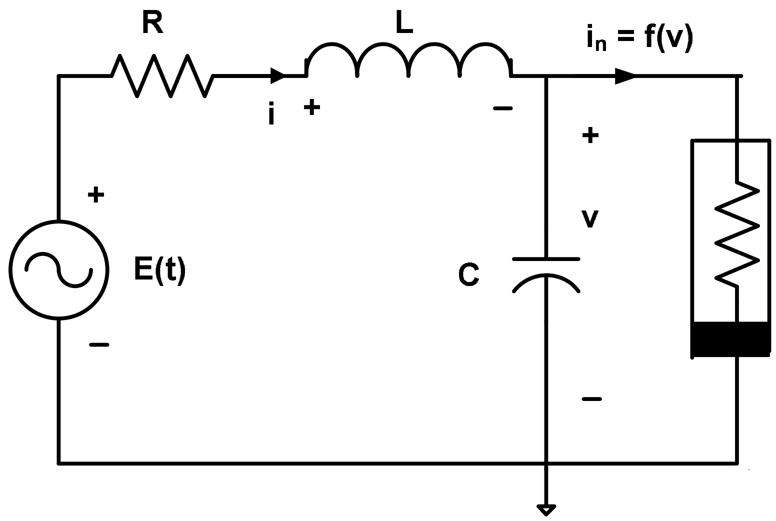

Figure 1: MLC Circuit.

2 Derivation of Equations and Hopf Bifurcations

In this section, we use the so-called MLC (Murali-Lakshmanan-Chua) circuit [Murali *et al.*, 1994b,a] as shown in Fig. 1 to study a new mechanism of creating chaotic attractors. As a simple second-order, dissipative, nonautonomous system, MLC circuit has been the subject of various studies [Murali *et al.*, 1994b,a; Lacy, 1996; Thamilmaran *et al.*, 2000; Aziz-Alaoui, 1999; Sen, 2001]. It has also been used in various chaotic communications, and chaos control schemes [Kılıç & Alçı, 2001; Okşaşoğlu

& Akgül, 1997; Ge & Wang, 2000]. In our investigation, the piecewise-linear $v - i$ characteristic of the nonlinear resistor in Fig. 1 is assumed to be replaced with a cubic polynomial. The governing set of dimensionless differential equations for this circuit can be given as

$$\begin{aligned}\frac{dx}{dt} &= \alpha[y - f(x)] \\ \frac{dy}{dt} &= -\beta[x + \gamma y] + \varepsilon P_T(t)\end{aligned} \tag{2}$$

where

$$\begin{aligned} &\alpha, \beta, \gamma \in \mathbb{R}^+ \\ f(x) &= b_1 x + b_2 x^2 + b_3 x^3 \\ P_T(t) &= \begin{cases} \sum_{k=-\infty}^{\infty} \delta(t - kT) & P1 \text{ type forcing} \\ \frac{1}{p} \sum_{k=-\infty}^{\infty} [u(t - kT) - u(t - kT - p)] & P2 \text{ type forcing} \end{cases} \end{aligned} \tag{3}$$

with $u(\cdot)$ being the unit step, and $\delta(\cdot)$ the impulse function. Here the dimensionless state variables x and y correspond to the capacitor voltage and the inductor current in Fig. 1, respectively, under proper transformations.

Let us rewrite Eq. (2) as

$$\frac{d}{dt}\begin{bmatrix} x \\ y \end{bmatrix} = \begin{bmatrix} -\alpha b_1 & \alpha \\ -\beta & -\beta\gamma \end{bmatrix} \begin{bmatrix} x \\ y \end{bmatrix} + \begin{bmatrix} -b_2 \alpha x^2 - b_3 \alpha x^3 \\ 0 \end{bmatrix} + \varepsilon \begin{bmatrix} 0 \\ 1 \end{bmatrix} P_T(t). \tag{4}$$

To get into a scenario of Hopf bifurcation, we let β vary around

$$\beta_0 = -\frac{\alpha b_1}{\gamma} > 0. \tag{5}$$

For $\beta > \beta_0$ sufficiently close to β_0, $p_0 = (0, 0)$ is an asymptotically stable equilibrium point. As β changes passing β_0, p_0 becomes unstable but a weakly stable periodic solution emerges from p_0. At $\beta = \beta_0$, Eq. (4) has a pair of purely imaginary eigenvalues $\pm i\omega$ with

$$\omega^2 = -\frac{\alpha^2 b_1}{\gamma}(1 + \gamma b_1) > 0 \tag{6}$$

which implies that

$$b_1 \in (-\frac{1}{\gamma}, 0). \tag{7}$$

To convert the linear part of Eq. (4) into the standard Jordan form we let

$$\begin{bmatrix} x \\ y \end{bmatrix} = \begin{bmatrix} 1 & 0 \\ b_1 + \frac{\sigma}{\alpha} & -\omega/\alpha \end{bmatrix} \begin{bmatrix} \xi \\ \eta \end{bmatrix}. \tag{8}$$

From this point on, all computations are performed at $\beta = \beta_0$. In terms of the new variables ξ and η, Eq. (4) becomes

$$\begin{aligned} \frac{d\xi}{dt} &= -\omega\eta - \alpha(b_2\xi^2 + b_3\xi^3) \\ \frac{d\eta}{dt} &= \omega\xi - \frac{\alpha^2 b_1}{\omega}(b_2\xi^2 + b_3\xi^3) - \varepsilon\frac{\alpha}{\omega}P_T(t). \end{aligned} \tag{9}$$

We now consider the autonomous part of Eq. (9), and compute the central manifold and the normal form. Note that in this case the whole space is the central manifold. If we define $z = \xi + i\eta$, then we obtain

$$\frac{dz}{dt} = i\omega z + h(z, \bar{z}) = i\omega z - \frac{\alpha}{8}[1 + i\frac{\alpha b_1}{\omega}][2b_2(z + \bar{z})^2 + b_3(z + \bar{z})^3]. \tag{10}$$

Now we use the formula given in [Guckenheimer & Holmes, 1997] to compute the normal form coefficient k_1. That is,

$$k_1 = \frac{i}{2\omega}(h_{zz}h_{z\bar{z}} - 2|h_{z\bar{z}}|^2 - \frac{1}{3}|h_{\bar{z}\bar{z}}|^2) + \frac{1}{2}h_{zz\bar{z}}. \tag{11}$$

Thus, following the notations in [Wang & Oksasoglu, 2005], we find that

$$
\begin{aligned}
-E(0)|_{\beta_0} &= \Re k_1 = \frac{\alpha}{8(1+\gamma b_1)}[2\gamma b_2^2 - 3b_3(1+\gamma b_1)] \\
F(0)|_{\beta_0} &= \Im k_1 = \frac{\alpha^2}{24\omega(1+\gamma b_1)}[2b_2^2(3\gamma b_1 - 2) - 9b_1 b_3(1+\gamma b_1)].
\end{aligned}
\tag{12}
$$

Equation (12) implies that for stability, we must have

$$
2\gamma b_2^2 - 3b_3(1+\gamma b_1) < 0. \tag{13}
$$

According to the theory (see [Wang & Oksasoglu, 2005]), we need to set

$$
\left|\frac{F(0)}{E(0)}\right| = \frac{\alpha}{3\omega}\left|\frac{b_1(9b_3\omega^2 + 10\alpha^2 b_2^2 b_1) + 4b_2^2\omega^2}{2\alpha^2 b_2^2 b_1 + 3b_3\omega^2}\right| \tag{14}
$$

large to obtain chaotic attractors.

3 Numerical Simulations

3.1 $P1$ Type Forcing

In this subsection, we present the results of numerical simulations for Eq. (2) with $P_T(t) = \sum_{n=-\infty}^{\infty} \delta(t - nT)$. This simulation is performed using the fourth-order Runge-Kutta routine starting at $t_0 = 0^+$. Integrating Eq. (2) consists of (i) integrating its autonomous part from $t = kT$ to $t = (k+1)T$, then (ii) changing the value of $x((k+1)T)$ to $x((k+1)T) + \varepsilon$. Note that care must be taken in selecting the integration step size. Throughout this section, the figures presented are the time-T maps of Eq. (2) with

$$(\alpha,\ \gamma,\ b_1,\ b_2,\ b_3,\ \beta,\ T) = (10.0,\ 1.0,\ -0.1,\ 1.15,\ 1.0,\ 0.99,\ 29.5). \tag{15}$$

In Eq. (15), our choice of T is quite arbitrary provided that it is "large" to afford us a long relaxation period between consecutive kicks of the external force. Note that with the fixed parameter values given in Eq. (15), we keep $F(0)/E(0)$ constant while satisfying the stability criterion of Eq. (13).

The limit cycle emerging from the center of a Hopf bifurcation for the autonomous part of Eq. (2), i.e., when $\varepsilon = 0$, is depicted in Fig. 2.

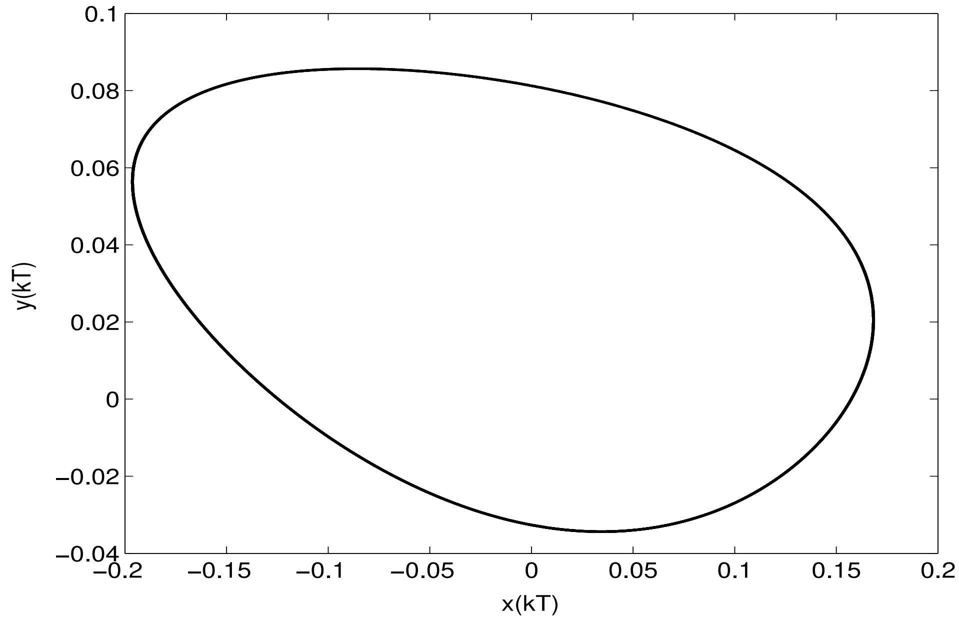

Figure 2: A Hopf Limit Cycle ($\varepsilon = 0.0$).

To obtain Figs. 3-5, we vary only ε. A chaotic attractor is observed at $\varepsilon = 0.04$, as depicted in Fig. 3. At $\varepsilon = 0.052$, we obtain a picture of a periodic sink as shown in Fig. 4. At $\varepsilon = 0.06$, we obtain another strange attractor as shown in Fig 5. Clearly, the two chaotic attractors that occur in Fig. 3 and Fig. 5 are different, meaning that they are not dynamically conjugate.

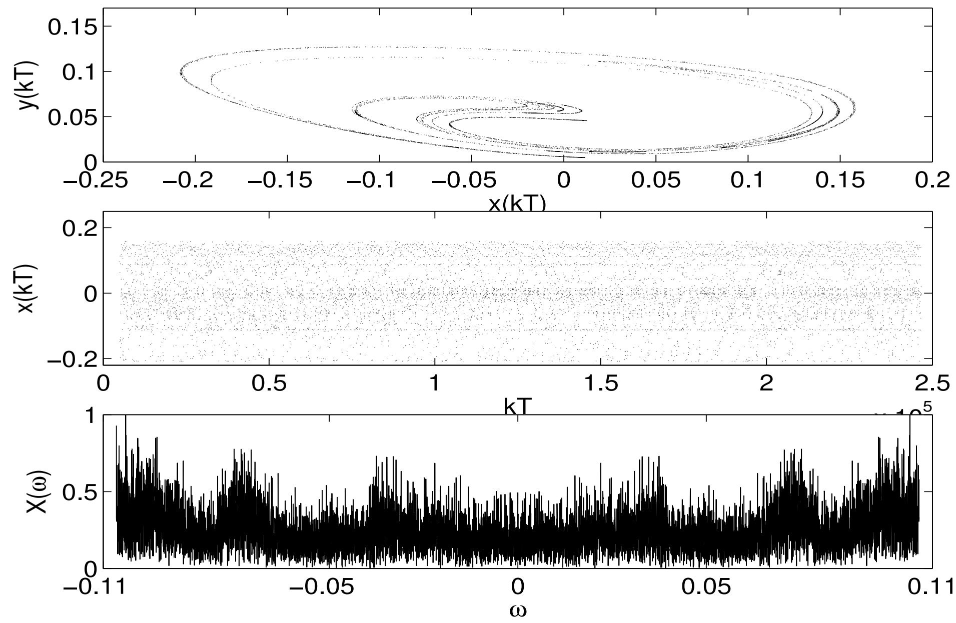

Figure 3: Strange attractor with $P1$ type forcing, $\varepsilon = 0.04$. Time-T map (top), x component of time-T map versus kT (middle), and frequency spectrum of $x(kT)$ (bottom).

Our simulations indicate that, in parameter space, stable periodic sinks and chaotic attractors are the two competing dynamical scenarios. This is consistent with the theoretical discussion given in [Wang & Oksasoglu, 2005].

3.2 $P2$ Type Forcing

In this subsection, we present the results of our numerical simulations for the system of Eq. (2) with $P_T(t) = P_{p,T}(t)$. Here, in addition to keeping all the parameter values same as in Eq. (15), we set $p = 0.5$, and vary ε.

As can be seen from Figs. 6-8, the results obtained are similar to those presented in Section 3.1.

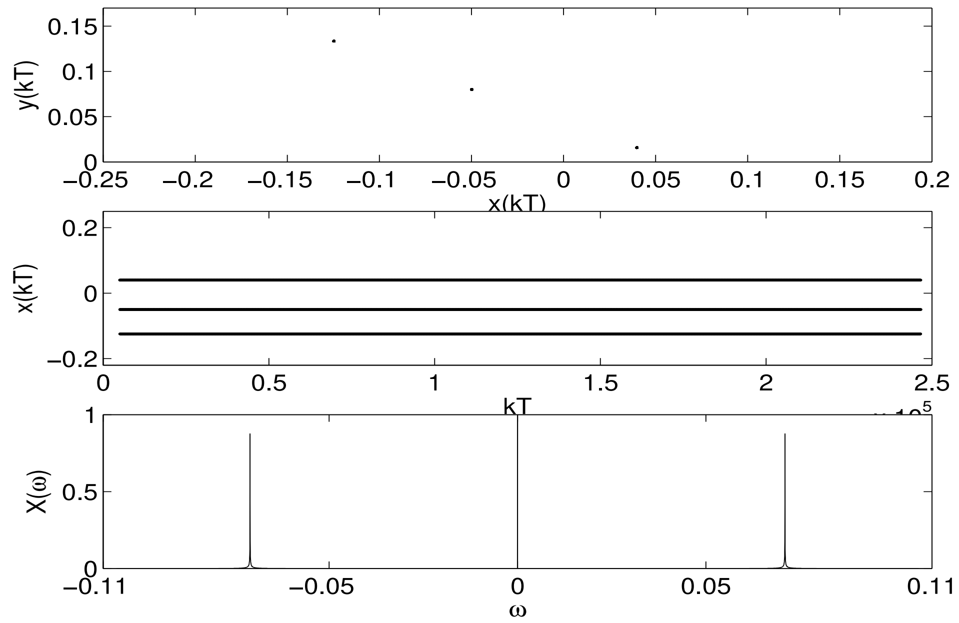

Figure 4: Periodic sink with $P1$ type forcing $\varepsilon = 0.052$. Time-T map (top), x component of time-T map versus kT (middle), and frequency spectrum of $x(kT)$ (bottom).

4 Other Considerations

4.1 Other Types of Forcing

Even though the theoretical results of [Wang & Young, 2002a] and [Wang & Young, 2004] were obtained for the $P1$ and $P2$ types of forcing, intuition suggests that the shape of the pulse should not play an important role in our scheme of producing strange attractors, provided that the relaxation period T is large enough.

To investigate this, we apply the waveform, which we call $P3$ type, shown in Fig. 9 to the system of Eq. (2). In this case, the forcing function is given, in its dimensionless form, by

$$P_{p,T}(t) = \frac{\pi}{2p} \sum_{n=-\infty}^{\infty} |\sin \frac{\pi}{p}(t - nT)|[u(t - nT) - u(t - nT - p)]. \tag{16}$$

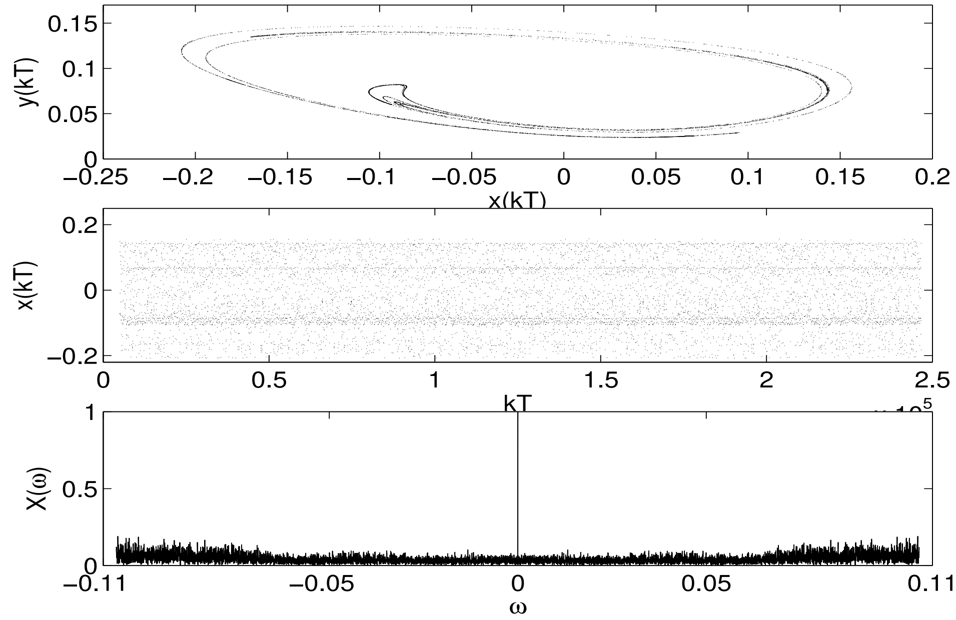

Figure 5: Strange attractor with $P1$ type forcing $\varepsilon = 0.06$. Time-T map (top), x component of time-T map versus kT (middle), and frequency spectrum of $x(kT)$ (bottom).

The constant term in Eq. (16) is so chosen that the area under the curve within one period is unity. Again, here we keep p constant at $p = 0.5$ in our simulations. As can be seen from Figs. 10-12, the simulation results of this section are in agreement with those of Sects. 3.1 and 3.2.

4.2 Non-Hopf Limit Cycles

The theoretical results proven in [Wang & Young, 2002a] are also applicable to limit cycles that do not necessarily emerge from Hopf bifurcations. To illustrate this, we consider the following parameter values for the system of Eq. (2):

$$(\alpha, \gamma, \beta, b_1, b_2, b_3, \varepsilon) = (10.0,\ 1.0,\ 0.995,\ -0.1,\ 1.5,\ 1.0,\ 0.0) \tag{17}$$

It can easily be verified from the stability criterion of Eq. (13) that, for these

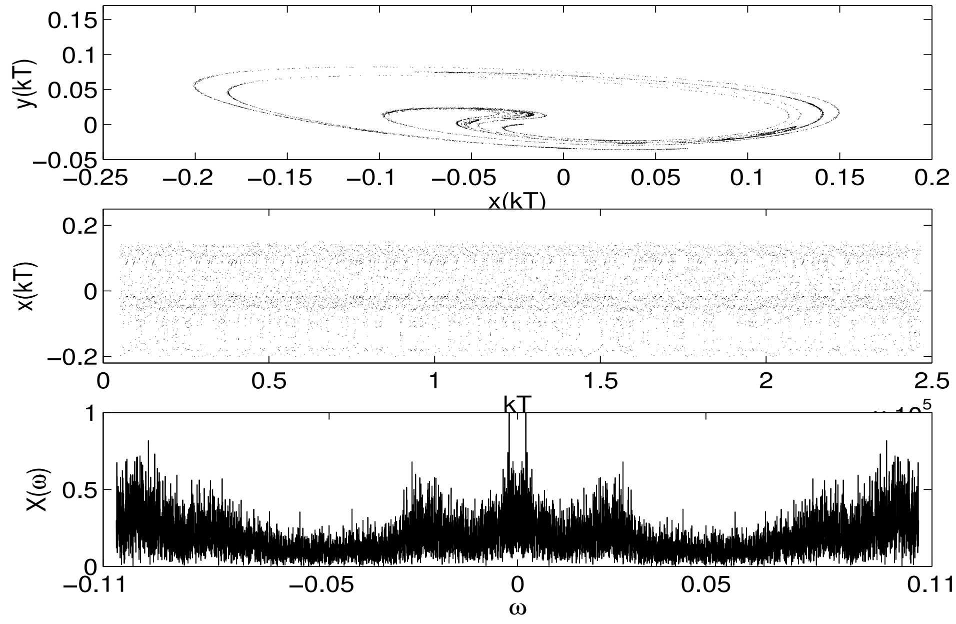

Figure 6: Strange attractor with $P2$ type forcing $\varepsilon = 0.04$. Time-T map (top), x component of time-T map versus kT (middle), and frequency spectrum of $x(kT)$ (bottom).

parameter values, the Hopf limit cycle around the origin is unstable. However, the system of Eq. (2), in this case, possesses a larger stable limit cycle as shown in Fig. 13. Now, to obtain strange attractors, we perturb the system of Eq. (2) by invoking $P1$, $P2$, and $P3$ types of forcing with

$$\varepsilon = 0.046, \quad T = 27.55 \quad p = 0.5 \; (P2 \text{ and } P3 \text{ types only}). \tag{18}$$

The other parameters are kept the same as in Eq. (17). The simulation results for the parameter values given in Eqs. (17) and (18) are illustrated in Figs. 14, 15, and 16 for the $P1$, $P2$, and $P3$ types of forcing, respectively.

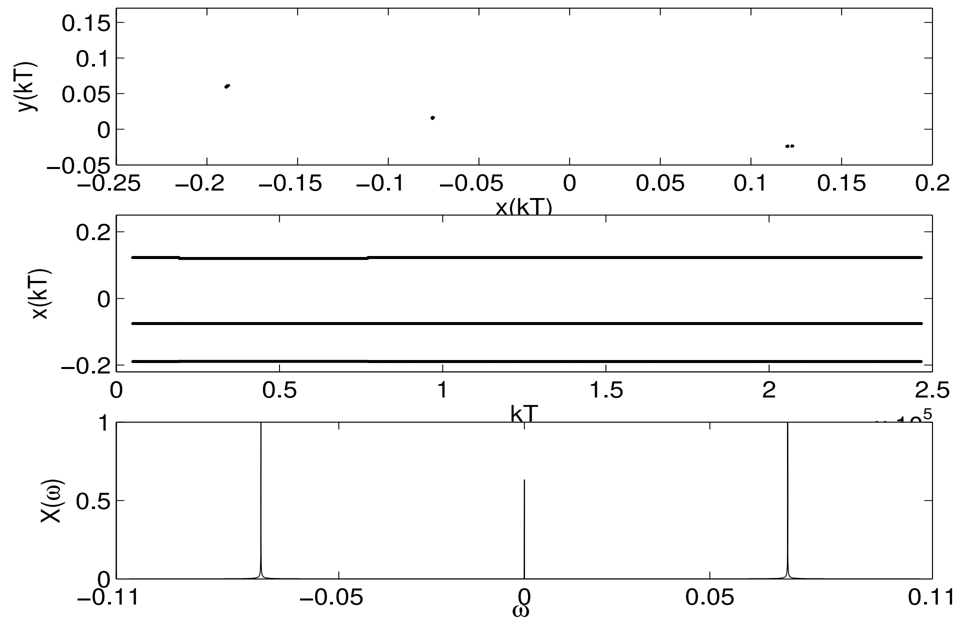

Figure 7: Periodic sink with $P2$ type forcing $\varepsilon = 0.0585$. Time-T map (top), x component of time-T map versus kT (middle), and frequency spectrum of $x(kT)$ (bottom).

5 Conclusion

In this paper, various types of periodic pulses, characterized by short pulse widths and long relaxation periods, are applied to the well-known MLC circuit to create rank one chaotic attractors under the guidance of a mathematical theory of rank one attractors recently developed. These periodic pulses are applied to weakly stable limit cycles emerging from Hopf bifurcations as well as to non-Hopf limit cycles. Various types of periodic pulses have been used to demonstrate that the same chaos-generating mechanism works for a variety of external forces. This important aspect of the theory indicates that in creating strange attractors this way the shape of the pulse is not crucial as long as there is a long enough relaxation period. However, the importance of using P1 and P2 types lies in the fact that it is possible, in this case, to explicitly compute the time-T map for the system of Eq. (1). Together with the work

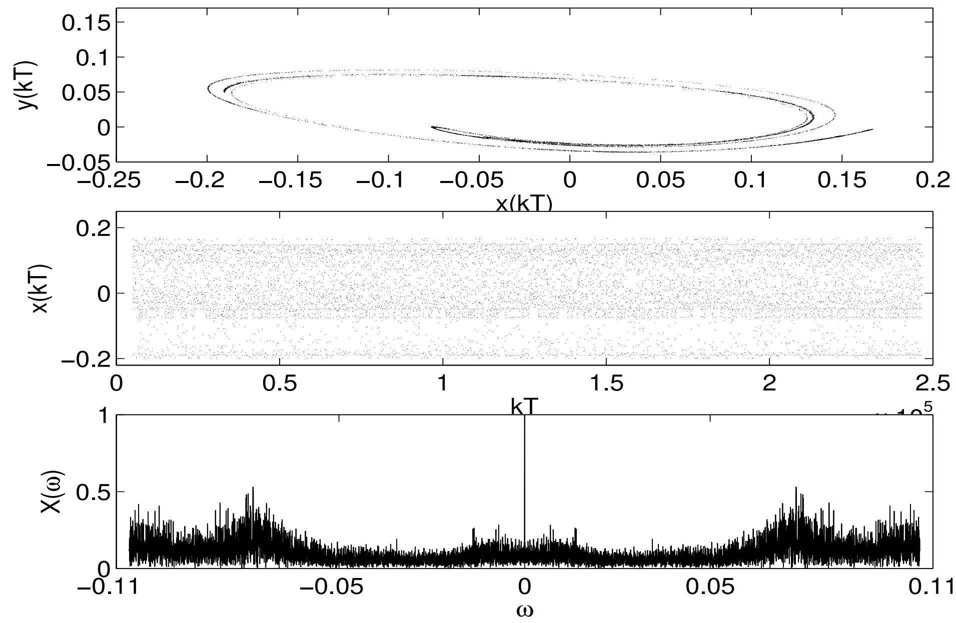

Figure 8: Strange attractor with $P2$ type forcing $\varepsilon = 0.068$. Time-T map (top), x component of time-T map versus kT (middle), and frequency spectrum of $x(kT)$ (bottom).

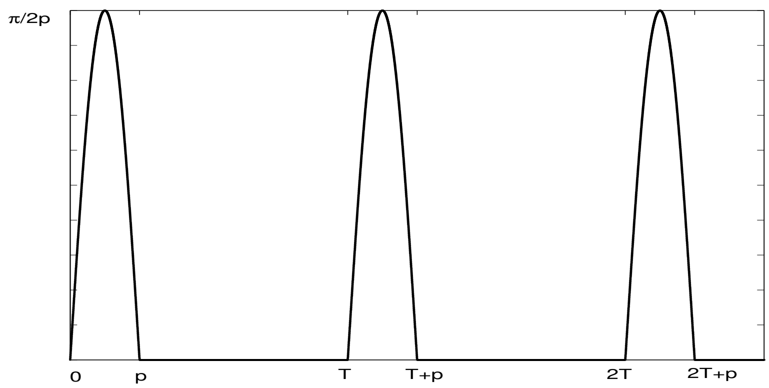

Figure 9: Pulsed Sine Wave.

presented previously in [Wang & Oksasoglu, 2005], we hope that this study leads to a wide variety of potential applications of the newly proposed mechanism.

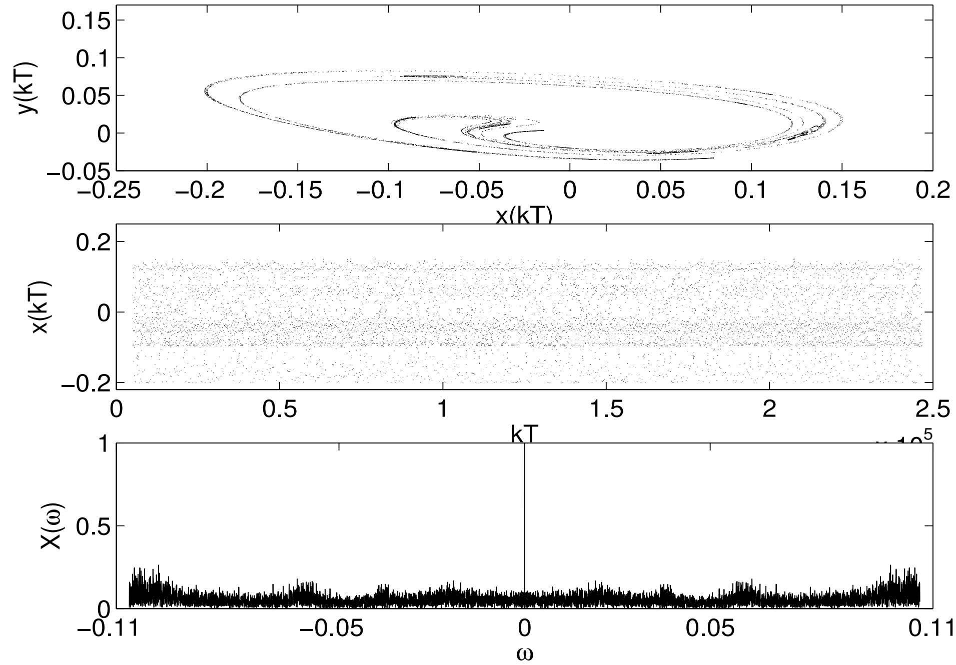

Figure 10: Strange attractor with $P3$ type forcing $\varepsilon = 0.04$. Time-T map (top), x component of time-T map versus kT (middle), and frequency spectrum of $x(kT)$ (bottom).

References

Aziz-Alaoui, M. A. [1999] "Differential equations with multispiral attractors," *Int. J. Bifurc. Chaos* **9**(6), 1009–1039.

Benedicks, M. & Carleson, L. [1991] "The dynamics of the Hénon map," *Ann. Math.* **133**, 73–169.

Benedicks, M. & Young, L.-S. [1993] "Sinai-Bowen-Ruelle measure for certain Hénon maps," *Invent. Math.* **112**, 541–576.

Chua, L. O., Komuro, M., & Matsumoto, T. [1986] "The double scroll family," *IEEE Trans. Circuits Syst. I* **33**(11), 1072–1118.

Elwakil, A. S. [2002] "Nonautonomous pulse-driven chaotic oscillator based on chua's circuit," *Microelectron J.* **33**, 479–486.

Ge, S. S. & Wang, C. [2000] "Adaptive control of uncertain chua's circuits," *IEEE Trans. Circuits Syst. I* **47**(9), 1397–1402.

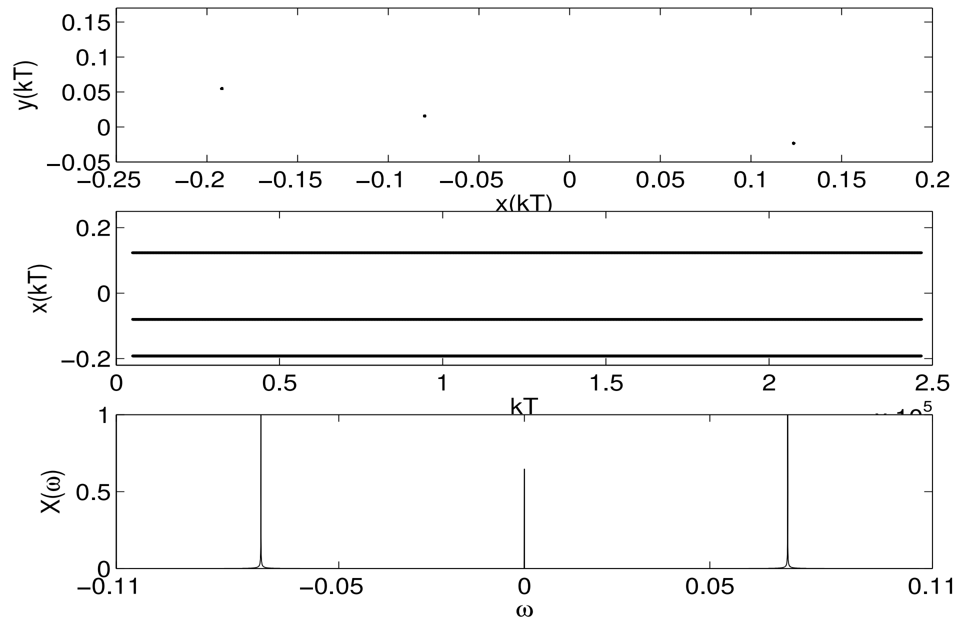

Figure 11: Periodic sink with $P3$ type forcing $\varepsilon = 0.056$. Time-T map (top), x component of time-T map versus kT (middle), and frequency spectrum of $x(kT)$ (bottom).

Guckenheimer, J. & Holmes, P. [1997] *Nonlinear Oscillations , Dynamical Systems and Bifurcations of Vector Fields* page 155 Applied Mathematical Sciences. Springer-Verlag New York fifth edition.

Jakobson, M. [1981] "Absolutely continuous invariant measures for one-parameter families of one-dimensional maps," *Commun. Math. Phys.* **81**, 39–88.

Kılıç, R. & Alçı, M. [2001] "Mixed-mode chaotic circuit and its application to chaotic communication for transmission of analog signals," *Int. J. Bifurc. Chaos* **11**(2), 571–581.

Lacy, J. G. [1996] "A simple piecewise-linear nonautonomous circuit with chaotic behavior," *Int. J. Bifurc. Chaos* **6**(11), 2097–2100.

Madan, R. N. [1993] *Chua's Circuit: A Paradigm for Chaos* World Scientific Singapore.

Miyachi, K., Nakano, H., & Saito, T. [2003] "Response of a simple dependent switched capacitor circuit to a pulse-train input," *IEEE Trans. Circuits Syst. I* **50**(9), 1180–1187.

Murali, K., Lakshmanan, M., & Chua, L. O. [1994a] "Bifurcation and chaos in the simplest dissipative nonautonomous circuit," *Int. J. Bifurc. Chaos* **4**(6), 1511–1524.

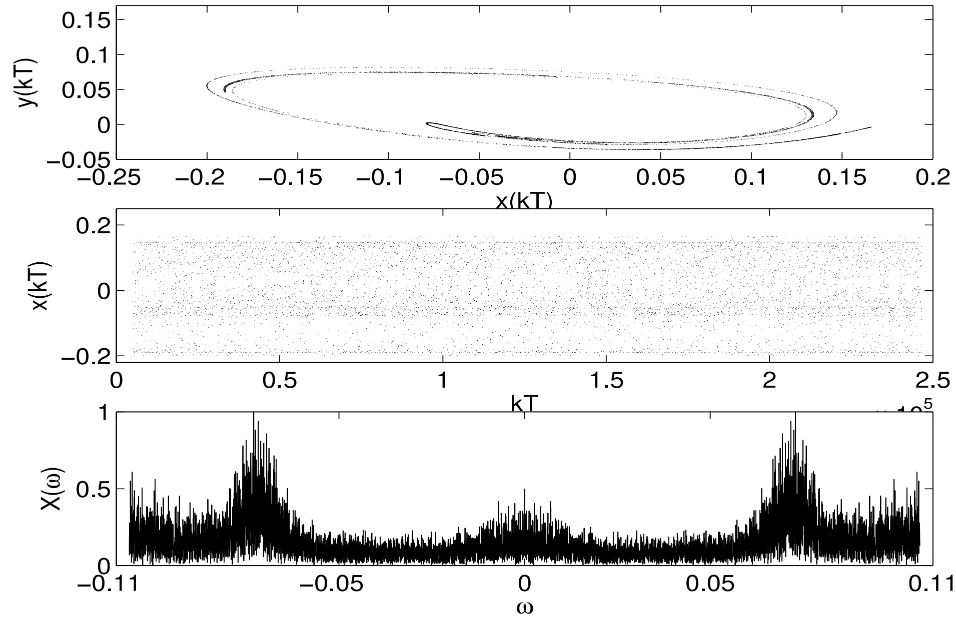

Figure 12: Strange attractor with $P3$ type forcing $\varepsilon = 0.064$. Time-T map (top), x component of time-T map versus kT (middle), and frequency spectrum of $x(kT)$ (bottom).

Murali, K., Lakshmanan, M., & Chua, L. O. [1994b] "The simplest dissipative nonautonomous chaotic circuit," *IEEE Trans. Circuits Syst. I* **41**(6), 462–463.

Okşaşoğlu, A. & Akgül, T. [1997] "A linear inverse system approach in the context of chaotic communications," *IEEE Trans. Circuits Syst. I* **44**(1), 75–79.

Özoguz, S. & Elwakil, A. S. [2004] "On the realization of circuit-independent nonautonomous pulse-excited chaotic oscillator circuits," *IEEE Trans. Circuits Syst. II* **51**(10), 552–556.

Sen, A. K. [2001] "An experimental study of nonlinear dynamics and chaos in a nonautonomous electronic circuit," *Int. J. Bifurc. Chaos* **11**(2), 583–589.

Stojanovski, T., Kocarev, L., & Parlitz, U. [1996] "Driving and synchronizing by chaotic impulses," *Phys. Rev. E.* **43**(9), 782–785.

Thamilmaran, K., Lakshmanan, M., & Murali, K. [2000] "Rich variety of bifurcations and chaos in a variant of murali-lakshmanan-chua circuit," *Int. J. Bifurc. Chaos* **10**(7), 1781–1785.

Wang, Q. & Oksasoglu, A. [2005] "Strange attractors in periodically kicked Chua's circuit," *Int. J. Bifurc. Chaos* **16**(1), 000–000.

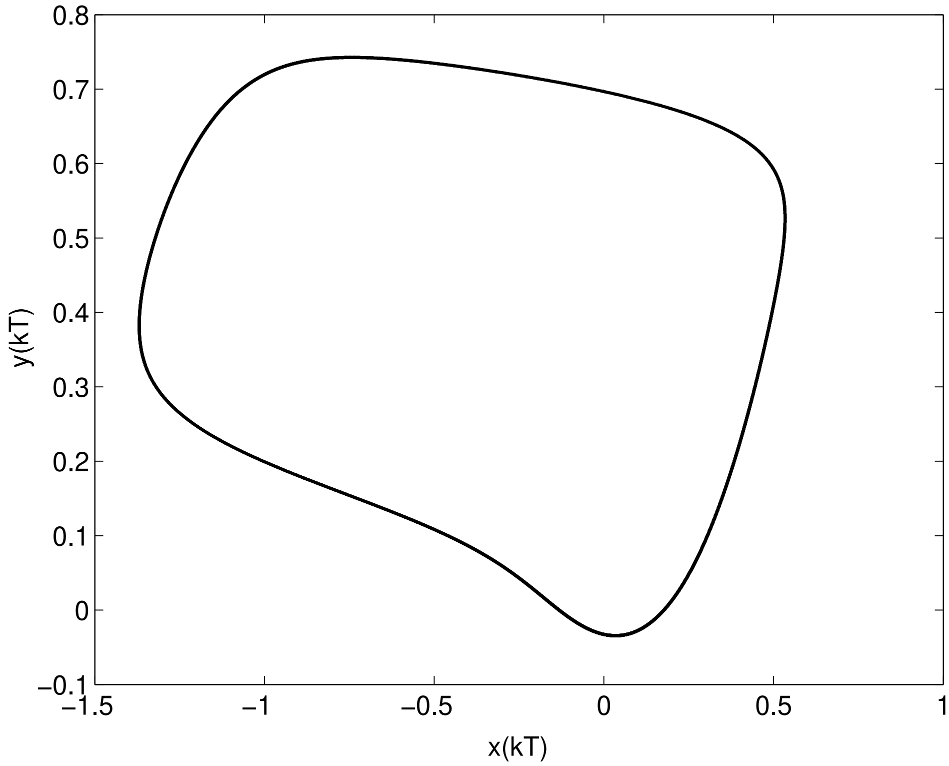

Figure 13: A Non-Hopf Limit Cycle.

Wang, Q. & Young, L.-S. [2001] "Strange attractors with one direction of instability," *Commun. Math. Phys.* **218**, 1–97.

Wang, Q. & Young, L.-S. [2002a] "From invariant curves to strange attractors," *Commun. Math. Phys.* **225**, 275–304.

Wang, Q. & Young, L.-S. [2002b] "Strange attractors in periodically-kicked limit cycles and Hopf bifurcations," *Commun. Math. Phys.* **240**, 509–529.

Wang, Q. & Young, L.-S. [2004] "Strange attractors emerging from from Hopf bifurcations," *In preprint.*

Wang, Q. & Young, L.-S. [2005] "Toward a theory of rank-one attractors," *To appear, Ann. Math.*

Yang, T. & Chua, L. O. [1997] "Impulsive control and synchronization of nonlinear dynamical systems and applications to secure communication," *Int. J. Bifurc. Chaos* **7**(3), 645–664.

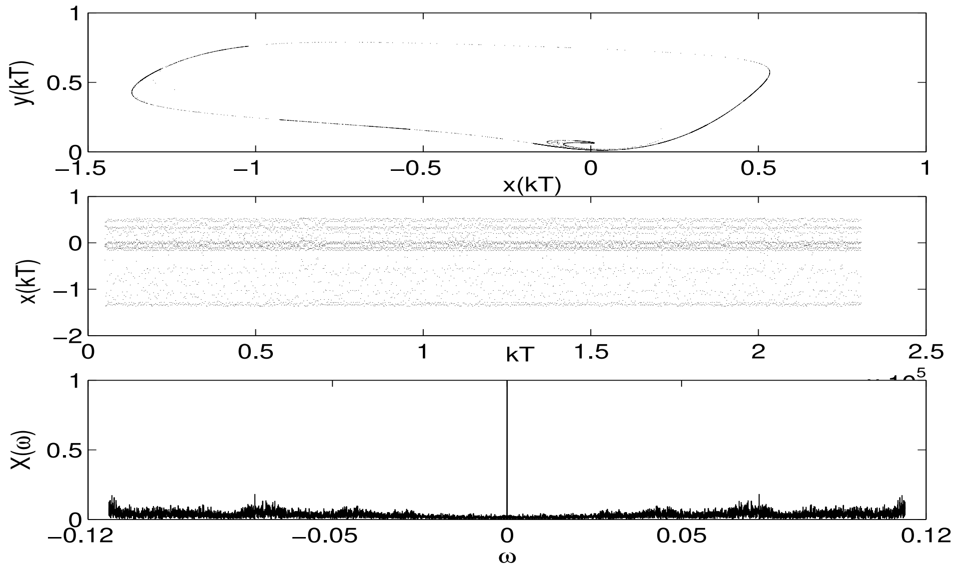

Figure 14: Strange attractor with $P1$ Type Forcing of a non-Hopf limit cycle. Time-T map (top), x component of time-T map versus kT (middle), and frequency spectrum of $x(kT)$ (bottom).

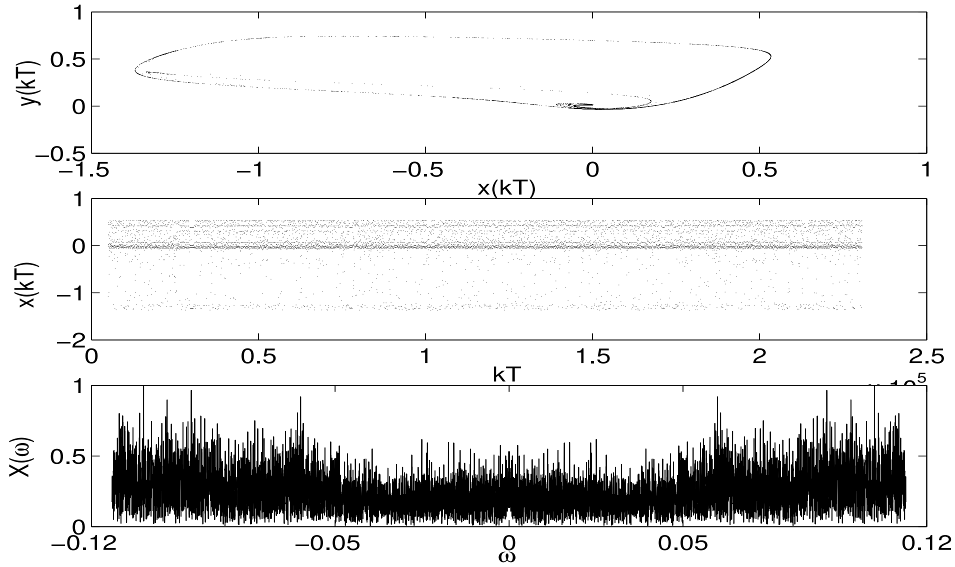

Figure 15: Strange attractor with $P2$ Type Forcing of a non-Hopf limit cycle. Time-T map (top), x component of time-T map versus kT (middle), and frequency spectrum of $x(kT)$ (bottom).

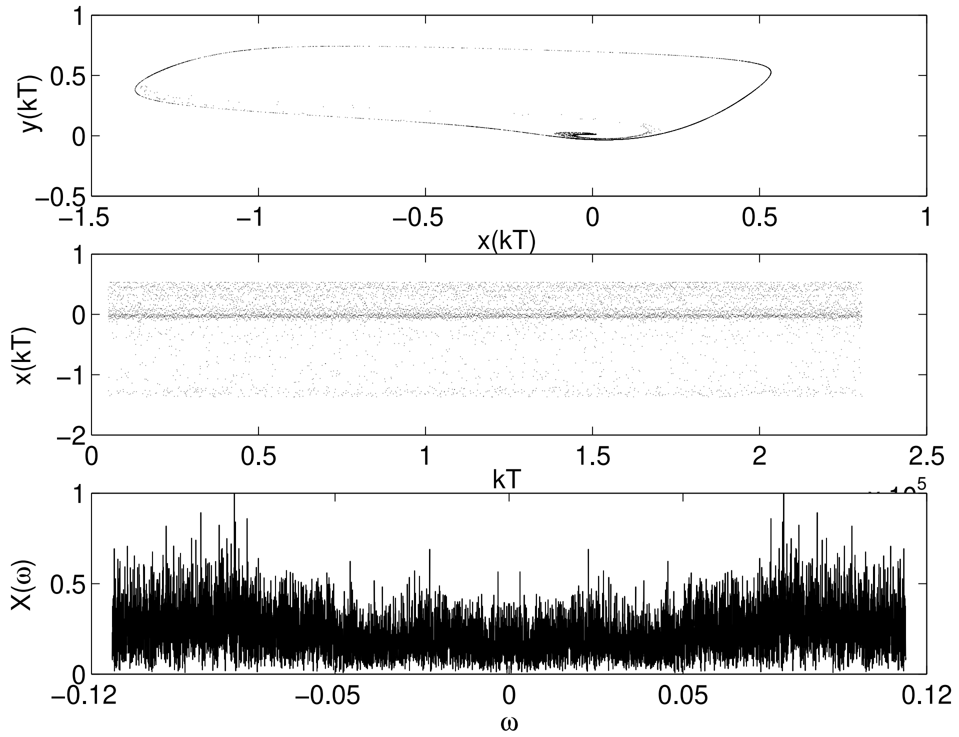

Figure 16: Strange attractor with $P3$ Type Forcing of a non-Hopf limit cycle. Time-T map (top), x component of time-T map versus kT (middle), and frequency spectrum of $x(kT)$ (bottom).